# TOWARD QUANTITATIVE VIRTUAL ANGIOGRAPHY: EVALUATION WITH *IN VITRO* STUDIES

*Jerome Durant*[1,2], *Irina Waechter*[3], *Roel Hermans*[4], *Juergen Weese*[1], *and Til Aach*[2]

[1] Philips Research Europe, Aachen, Germany
[2] Institute of Imaging and Computer Vision, RWTH Aachen University, Aachen, Germany
[3] Centre for Medical Image Computing, University College London, UK
[4] Philips Medical Systems, X-ray Pre-Development, Best, the Netherlands

## ABSTRACT

Medical imaging and computational fluid dynamics (CFD) modeling have been combined to obtain detailed knowledge of local hemodynamics, known to play an important role in cardiovascular diseases. Given the absence of a "gold standard" to measure the blood velocities *in vivo*, simulation of X-ray angiograms was proposed as a method to indirectly validate the accuracy of image-based CFD analysis. This paper presents a method to simulate the contrast agent transport and the creation of virtual angiograms which takes into account the physics of the contrast agent injection and X-ray transmission. The simulated and acquired angiograms are compared by analyzing the spatial and temporal development of the contrast agent concentration represented by a flow map. This approach was tested with *in vitro* experiments.

***Index Terms***— X-ray imaging, virtual angiography, medical image-based simulation, blood flow, computational fluid dynamics

## 1. INTRODUCTION

Local hemodynamics plays an important role in cardiovascular diseases such as atherosclerosis - the principal cause of mortality in the western world - and the growth and rupture of aneurysms. As no method is currently available to accurately measure the flow patterns *in vivo*, the exact nature of blood flow is being assessed by coupling medical imaging techniques with computational fluid dynamics (CFD) analysis with a patient-specific approach. Over the past ten years, the accuracy and precision of image-based CFD modeling has been improved notably by refining the geometry extraction and the modeling of the blood characteristics.

Nevertheless, the accuracy of image-based CFD analysis is difficult to assess, given the absence of a "gold standard" to measure the blood velocities *in vivo*. Studies to check the accuracy of flow modeling with CFD have first relied on comparisons with *in vitro* measurements made in phantoms or casts. The *in vitro* studies showed that CFD can reliably model flow in realistic representations of arteries [1]. However, *in vitro* experimental validations do not prove that the CFD models are accurately reproducing the *in vivo* hemodynamics. Several studies have found good *qualitative* agreement between simulated and phase contrast MRI (PC-MRI) imaged *in vivo* flow patterns [1]. Coupling CFD to imaging physics modeling was proposed [2] to create "virtual" images which can directly be compared to the actual acquired images, and hence to validate indirectly the patient-specific simulations.

Interventional X-ray imaging is routinely used for the treatment of cardiovascular disease. For instance, the 3D vascular geometry can be reconstructed with rotational angiography (3D RA) and the local hemodynamics can be analyzed qualitatively with digital subtraction angiography (DSA) after a contrast agent injection. Simulation of contrast agent transport in the arterial system has been used so far to visualize [3,4] and to validate qualitatively [2,5] the simulated flow dynamics. From the simulated contrast agent transport, few studies looked at the creation of simulated angiograms which could imitate real angiograms. Cebral *et al.* used either surface plots or volume rendering techniques to create images called "virtual angiograms" [5]. Ford *et al.* [2] took into account the physics of X-ray transmission by calculating the attenuation of the X-ray photons travelling through the computational model after interpolating the contrast agent concentration results in a structured grid. However, because of a low X-ray acquisition frame rate (2 Hz), the temporal resolution of their angiogram sequences was limited.

In this paper, we extend the study of Ford *et al.* and propose a method to create the virtual angiograms by modeling the physics of the contrast agent injection and X-ray transmission and we assess the effect of different modeling parameters on the virtual angiogram creation. We use a comprehensive way to compare the spatial and temporal development of contrast agent concentration by representing it with a flow map [6]. The validation of the approach was performed with *in vitro* X-ray experiments with a straight tube and a bifurcation.

## 2. MATERIALS AND METHODS

### 2.1. Experimental setup

The setup [6] is composed of a pulsatile flow circuit, a clinical contrast agent injector (MarkVProVis, Medrad), and a rotational X-ray system (Allura Xper with a FD20 detector, Philips Medical Systems). Water was used to mimic the blood. The image acquisitions were performed with a frame rate of 30 Hz following an injection of contrast (Ultravist-370, Schering) into a straight tube or a glass phantom representing an idealized carotid bifurcation. Each phantom was placed in an elliptical, water filled cylinder-like container to generate realistic noise, beam hardening, and scatter. The ground truth flow was obtained with an electromagnetic flow meter (EMF).

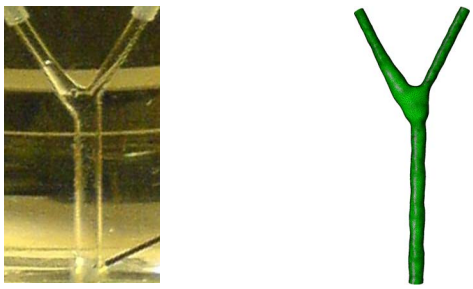

(a) (b)

**Fig. 1.** Glass phantom of an idealized carotid bifurcation (a) and its mesh reconstructed from 3D RA (b).

### 2.2. Construction of the geometric models for CFD

The straight tube phantom was modeled by a cylinder (30 mm length, 4 mm diameter) and a structured mesh was generated with 60,000 hexahedral elements. By comparing the simulation results with those obtained with a finer mesh, the mesh resolution was proven to be sufficient.

For the bifurcation glass phantom (Fig. 1.a), 3D RA images of the structure filled with contrast agent were acquired. The geometry was segmented with a simple thresholding technique and a triangulated mesh was generated. Planar boundaries were created at the mesh extremities with the help of the geometry centerline, to create proper boundary conditions for the simulations. Finally, an unstructured mesh of about 181,500 tetrahedral elements (Fig. 1.b) was created using Netgen (version 4.4, created by J. Schoeberl).

### 2.3. Flow simulation

The Navier-Stokes equations governing the time-dependent flow were solved with the open source program OpenFOAM (versions 1.3 or 1.4.1, OpenCFD Ltd) using parallel computing. The liquid (water) was assumed to be Newtonian and the flow to be laminar and incompressible. The kinematic viscosity of the water at 20°C ($10^{-6}$ m$^2$/s) was chosen.

A time-varying flow was set at the inlet and traction free boundary conditions were set at the outlets. The simulations converged to a periodic solution after a few cardiac cycles. For the time-varying non-periodic simulations, these results were used as initialization. The inlet flow waveform was derived from the EMF measurements (Fig. 2). Fully developed velocity profiles were set at the inlet. They were obtained from the Womersley solution as detailed in Cebral *et al.* [7]. No-slip boundary conditions were applied to the walls, which were assumed to be rigid.

### 2.4. Contrast agent simulation

*Modeling of the contrast agent transport*

As the contrast agent is commonly assumed to emulate the blood characteristics, its propagation can be modeled as a passive transport of particles within the blood with the following convection-diffusion equation [3,5]:

$$\frac{\partial C}{\partial t} + v \cdot \nabla C = \kappa \nabla^2 C \quad , \qquad (1)$$

where $C$ is the contrast concentration, $v$ is the velocity vector field and $\kappa$ the diffusivity constant. This assumption was also adopted for our modeling process, while, Kim and Ford *et al.* [2,4] used another convection-diffusion equation instead.

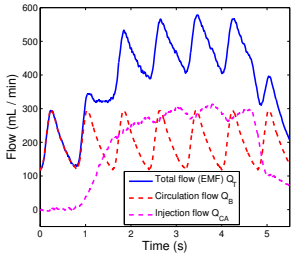


**Fig. 2.** Total flow from the EMF of an experiment and deduction of the circulation and injection flows.

The diffusion coefficient value $\kappa$ is difficult to determine. Kim *et al.* [4] used the fact that the diffusivity constant of urea in water is close to $10^{-9}$ m$^2$/s. As no ground truth is available for the diffusivity constant, simulations were performed with different values (typically between $10^{-6}$ and $10^{-10}$ m$^2$/s) and compared with each other.

For some simulations, the total flow was assumed to be periodic and the flow and contrast agent simulations were computed successively. The Navier-Stokes equations of the flow simulation are solved and the results of the last cardiac cycle are stored. As a periodic flow is assumed, the stored results are used for all the cardiac cycles of the contrast agent simulation performed by solving the transport equation.

The assumption of flow periodicity during the injection is valid in the human vasculature system, because of high downstream resistances. On the contrary, for the experimental set-up, the injection increases the total flow and the periodicity assumption becomes less realistic (Fig. 2). Therefore, the total flow from the EMF was used to model the flow increase at the inlet. The flow and the contrast agent simulations were calculated simultaneously to avoid saving numerous flow results over several periods.

*Boundary conditions and injection assumptions*

Iodine was the attenuation component of the contrast agent. A time-varying iodine concentration was applied at the inlet. Zero-gradient of concentration was set at the wall to avoid contrast transport through the wall and at the outlets to prescribe vanishing diffusive flux. In the experiments, the injection point was typically about 10 cm away from the region which was acquired.

In case of the experimental set-up, the injection flow is mainly added to the periodic flow. Thus, from the EMF measurements of the total flow $Q_T$, the information on the water flow waveform $Q_B$ and injection flow waveform $Q_{CA}$ can be deduced using $Q_T(t) = Q_B(t) + Q_{CA}(t)$ (Fig. 2) and the iodine concentration at the injection site is given by

$$C_I(t) = \frac{Q_{CA}(t)}{Q_T(t)} C_{I/CA} \quad , \qquad (2)$$

where $C_{I/CA}$ is the iodine concentration in the contrast agent.

The iodine concentration at the inlet can also be approximated from the acquired angiograms. This is the only method available in clinical studies. Unlike previous works [2,3] which modeled the inlet concentration with a gamma-variate function, no prior shape was assumed as it could be deduced from the X-ray acquisitions performed with a frame rate of 30 Hz. The concentration variations over time were obtained by analyzing the time intensity curves (TIC) in a small region of interest close to the inlet. Without additional calibration, the mean amplitudes of the TICs do not represent the actual concentration amplitudes.

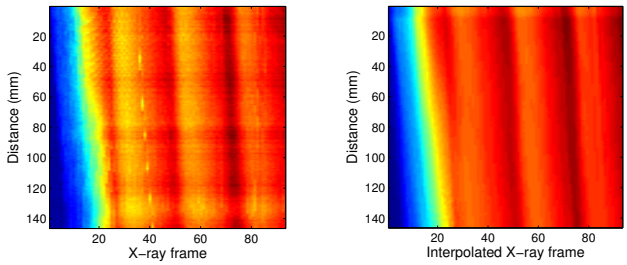


(a) (b)

**Fig. 3.** Flow maps from the straight tube study, (a) extracted from the *in vitro* experiments, (b) simulated assuming time-varying non-periodic flow (assuming $\kappa = 10^{-8}$ m$^2$/s and using the extracted TICs for the inlet concentration). The flow maps were compared with the same time scale with a frame rate of 30 Hz. Similar pulsatile patterns are clearly visible in both flow maps.

As proposed by Ford *et al.* [2], uniform mixing was assumed for the contrast agent distribution at the inlet; this is realistic if the inlet is located sufficiently far from the injection point. In addition, some simulations were performed with a parabolic distribution.

### 2.5. Virtual angiogram creation

For the creation of X-ray projection images, the concentration results stored at each cell center of the 3D mesh were interpolated onto a structured grid (volume of voxels). The voxel size was chosen according to the vessel radii. Three different sizes were tested: 0.5, 0.25 and 0.125 mm.

To create the projection images, the additional attenuation caused by the iodine in the contrast agent is of interest. The attenuation $\mu$ of the mixture of iodine and water for different energy levels $E$ of the spectrum can be calculated from the iodine concentration $C_I$ with

$$\mu(E, C_I) = \frac{C_I}{\rho_I}\,\mu_I(E) + (1 - \frac{C_I}{\rho_I})\,\mu_W(E) \quad , \qquad (3)$$

where $\mu_I$ is the iodine attenuation, $\rho_I$ the iodine density and $\mu_W$ the water attenuation.

The X-ray projections were created with the in house program Radonis (Philips Research Hamburg). It simulates the number of detected photons for each detector pixel. The X-ray spectrum, the current and the radiation time were specified. The tube and detector positions relative to the created volume were set to obtain a similar orientation as the acquired projections. Digital subtraction angiography (DSA) was obtained by subtracting an image without contrast agent from all the simulated images.

### 2.6. Flow map creation

As illustrated in Fig. 3, the flow map [6] is represented as an image, where the pixel intensity is proportional to the iodine concentration, the horizontal dimension is time and the vertical dimension is length along the vessel centerline. Flow maps allow the analysis of the image intensity variations in respect to time and distance along the projected vessel centerline. A good match of two flow maps is not only a necessary condition but also a good indication for a proper match between the corresponding two sets of angiograms.

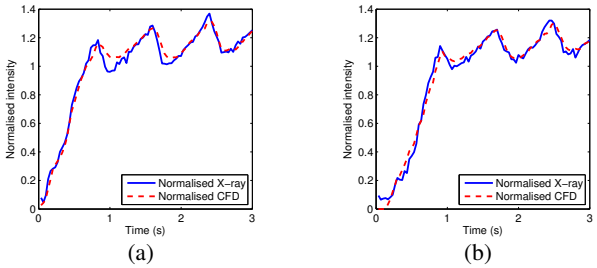


(a) (b)

**Fig. 4.** TICs from the straight tube study at (a) 60 mm and (b) 140 mm along the projected centerlines and corresponding to rows of the flow maps presented in Fig. 3.

## 3. RESULTS

The simulated flow maps were compared to the flow map extracted from the X-ray angiograms. For the straight tube study, the results for the finer voxel resolutions of 0.25 mm and 0.125 mm agreed very well with each other, only the coarse resolution of 0.5 mm was not consistent with these. Also, for the simulations with time-varying non-periodic flow in the straight tube, a better match was obtained than for the periodic flow (Fig. 3). After mean normalization of the two flow maps of Fig. 3, the mean relative error was less than 10%, the highest relative errors were located close to the bolus arrival of the contrast. Studying the TICs along the projected geometry centerlines (flow map rows) allow comparing visually the results (Fig. 4). The concentration variations due to the pulsatile nature of the flow are comparable.

The virtual angiograms created with the bifurcation glass phantom (Fig. 5) closely resemble the acquired angiograms and confirm that the method can be applied to complicated geometries. Fig. 5 shows that using flow maps allows better quantitative comparisons of the angiogram sequences. Preliminary comparisons of the flow maps for each branch demonstrated a good resemblance. The pulsatile pattern was not visible on the flow maps at the bifurcation location. Further investigations will compare the flow division at the bifurcation.

## 4. DISCUSSION

As illustrated in Fig. 3 and Fig. 4, a strong correspondence can generally be seen between simulated and extracted flow maps. To the best of our knowledge, this study shows the first comparisons of acquired with simulated angiograms with a high temporal resolution. Remaining deviations between the extracted and simulated angiograms can be explained by several factors from the CFD modeling to the creation of the X-ray projections.

A fluid viscosity is temperature dependent. Changing slightly the water viscosity did not have a significant impact on the flow map. However, the injection of dye with a higher viscosity than the water viscosity may need to be taken into account. The Womersley solution corresponds to a homogeneous, incompressible, Newtonian fluid flow in a rigid, long cylinder submitted to an arbitrary periodic waveform. As some of these assumptions are not fulfilled, some inaccuracies may be induced.

Variations in the contrast agent diffusion coefficient (from $10^{-10}$ m$^2$/s to $10^{-7}$ m$^2$/s) caused negligible differences in the flow map in case of high flow rate. However, with moderate flow rate, this caused significant changes at locations far from the injection point; hence, this constant should be approximated accurately.

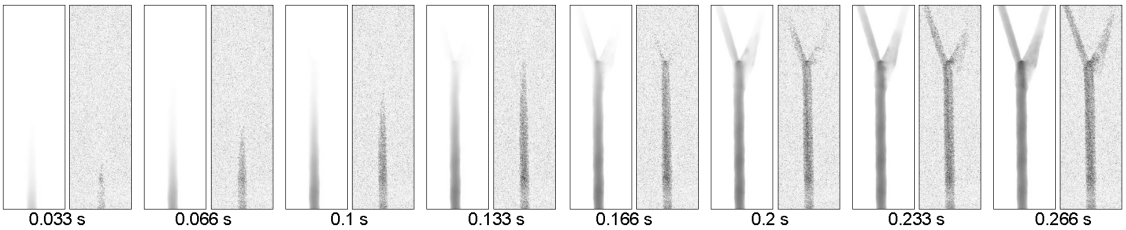


**Fig. 5.** Simulated (left) and acquired (right) subtracted angiograms corresponding to the contrast agent arrival in the bifurcation glass phantom. The time of each simulated projection was chosen as a multiple of the simulation time step close to the acquisition time.

Independently from the mesh resolution, the resolution of the volume of voxels was found to limit the total accuracy. Because of computer memory limitations, Ford *et al.* used a voxel size of 0.5 mm [2]. After comparing the results obtained with three different resolutions, 0.25 mm was chosen as a compromise between accuracy and computational requirements. Moreover, the interpolation from the mesh to the voxel volume may be improved to determine more accurate values at the voxel centers. Modeling the energy spectrum allowed obtaining a better mean attenuation of the flow map but did not change the concentration patterns.

Inaccuracies may also originate from the X-ray acquisition. For a monochromatic X-ray spectrum, the attenuation line integral is theoretically proportional to the logarithm of the normalized detector intensity. In practice, the acquired images need to be corrected for offset and gain, white compression, beam hardening, scatter and other effects in order to obtain the true line integrals. The processed images are called quantitative X-ray images. Instead, an iodine calibration can be beneficial to relate the image intensities to the iodine concentration. For the presented studies, as all the effects were not corrected, the mean amplitudes were slightly different between the simulated and extracted flow maps. Thus, the results were normalized before the comparisons.

For most of the simulations, the contrast agent mixing was assumed to be homogeneous across the inlet cross section. Using a parabolic inlet contrast agent distribution changed significantly the flow map. The distributions across the cross sections are in fact changing with time: because of the velocity profile, the dye arrives earlier at the vessel center than at the vessel borders. The injection protocol (e.g. catheter type, injection rate, injection point location) will influence the mixing and may induce turbulences. As the contrast agent density is higher than blood and water densities, the gravity can induce asymmetric mixing, particularly for *in vitro* experiments.

Unlike the previous studies, the x-ray acquisition frame rate of 30 Hz allowed obtaining a proper inlet contrast agent concentration, observing the flow patterns in the images, and comparing accurately virtual and acquired images. Further *in vitro* studies are planned, notably by using iodine calibration.

The extension of the presented method to clinical studies will require further refinements of the modeling process. The flow and contrast agent simulations will need to model the complex blood flow and vessel characteristics (e.g. moving walls, advanced outlet conditions). Ideally, the blood flow waveform of the patient will be acquired either with PC-MRI or Doppler ultrasound. As a substitute, a flow waveform of an age- and sex- matched control is commonly used. A proper time correspondence between the patient-specific flow waveform and the angiograms could be obtained if the injection is started at the peak blood flow rate. The influence of the injection on the total flow *in vivo* [2] may also need to be considered.

## 5. CONCLUSION

By providing a deeper knowledge of the 3D blood flow patterns, image-based CFD analysis may help the diagnostics and treatment of cardiovascular diseases. Virtual angiography can allow an indirect validation of this approach and provides a useful tool for visualizing complex CFD results. The present work has shown that, by modeling all the steps from the fluid and contrast agent transport to the physics of the X-ray transmission, virtual angiograms can be created and compared quantitatively with acquired angiograms. The use of flow maps provides a simple approach to compare an angiogram sequence acquired at different times. This work can pave the way to the creation of patient-specific virtual angiograms and their comparisons with the acquired angiograms.

## 6. ACKNOWLEDGMENTS

The authors thank Brian O'Neill (Philips Research Aachen) for his support with the parallel Linux cluster. This project received financial support from the European Union under contract MEST-CT-2005-020424.

## 7. REFERENCES

[1] D.A. Steinman, "Image-based computational fluid dynamics modeling in realistic arterial geometries". *Ann. Biomed. Eng.,* 30, pp. 483–497, 2002.

[2] M.D. Ford *et al*., "Virtual angiography for visualization and validation of computational fluid dynamics models of aneurysm hemodynamics", *IEEE Trans. Med. Imag.*, 24(12), pp. 1586-1592, 2005.

[3] F. Calamante *et al*., "Estimation of bolus dispersion effects in perfusion MRI using image-based computational fluid dynamics", *NeuroImage*, 19, pp. 342–353, 2003.

[4] T. Kim *et al*., "A simulated dye method for flow visualization with a computational model for blood flow", *J. Biomech.*, 37, pp. 1125–1136, 2004.

[5] J.R. Cebral *et al*., "Qualitative Comparison of Intra-aneurysmal Flow Structures determined from conventional and virtual angiograms", *Proc. SPIE Med. Imag.*, 6511, pp. 1E1-1E9, 2007.

[6] I. Waechter *et al.*, "Quantification of blood flow from rotational angiography", *MICCAI*, *LNCS*, 4791, pp. 634–641, 2007.

[7] J.R. Cebral *et al.*, "Efficient pipeline for image-based patient-specific analysis of cerebral aneurysm hemodynamics: Technique and sensitivity", *IEEE Trans. Med. Imag.*, 24(4), pp. 457-467, 2005.